LETTERS
PUBLISHED ONLINE: 7 DECEMBER 2015 | DOI: 10.1038/NCLIMATE2879
nature climate change

Large divergence of satellite and Earth system model estimates of global terrestrial CO_2 fertilization

W. Kolby Smith[1,2*], Sasha C. Reed[3], Cory C. Cleveland[1], Ashley P. Ballantyne[1], William R. L. Anderegg[4], William R. Wieder[5,6], Yi Y. Liu[7] and Steven W. Running[1]

Atmospheric mass balance analyses suggest that terrestrial carbon (C) storage is increasing, partially abating the atmospheric [CO_2] growth rate[1], although the continued strength of this important ecosystem service remains uncertain[2–6]. Some evidence suggests that these increases will persist owing to positive responses of vegetation growth (net primary productivity; NPP) to rising atmospheric [CO_2] (that is, 'CO_2 fertilization')[5–8]. Here, we present a new satellite-derived global terrestrial NPP data set[9–11], which shows a significant increase in NPP from 1982 to 2011. However, comparison against Earth system model (ESM) NPP estimates reveals a significant divergence, with satellite-derived increases (2.8 ± 1.50%) less than half of ESM-derived increases (7.6 ± 1.67%) over the 30-year period. By isolating the CO_2 fertilization effect in each NPP time series and comparing it against a synthesis of available free-air CO_2 enrichment data[12–15], we provide evidence that much of the discrepancy may be due to an over-sensitivity of ESMs to atmospheric [CO_2], potentially reflecting an under-representation of climatic feedbacks[16–20] and/or a lack of representation of nutrient constraints[21–25]. Our understanding of CO_2 fertilization effects on NPP needs rapid improvement to enable more accurate projections of future C cycle–climate feedbacks; we contend that better integration of modelling, satellite and experimental approaches offers a promising way forward.

Global trends in NPP have been difficult to characterize with observations and models, and remain an unresolved area of scientific research—hampered by the limited availability of long-term, large-scale data and an incomplete understanding of the variety of interacting feedbacks that regulate NPP. For example, rising atmospheric [CO_2] may enhance NPP by stimulating photosynthetic activity[5–8], resulting in an increase in intrinsic vegetation water use efficiency[8] (WUE). Yet, warmer climatic conditions resulting from rising [CO_2] may increase vegetation moisture stress, attenuating the direct positive effects of enhanced [CO_2] on NPP (refs 19,20). Adding complexity, the magnitude and duration of the direct positive effects of rising [CO_2] on NPP are thought to be constrained by nutrient availability, specifically the availability of nitrogen (N) and phosphorus (P), which play critical roles in regulating plant photosynthesis and growth[21,22]. Thus, long-term trends in NPP reflect a complex balance between multiple interacting biophysical (for example, temperature and water) and biogeochemical (for example, [CO_2] and nutrient) feedbacks.

ESMs face the difficult challenge of representing these potentially counteracting feedbacks in a realistic way. The comprehensive ESMs that participated in the Fifth Coupled Model Intercomparison Project (CMIP5) represent our collective best approximation of future global C dynamics, and thus have been used to define critical policy targets, such as future allowable anthropogenic CO_2 emissions[2,3]. Some have questioned the validity of these projections, often citing model oversimplifications or missing C cycle feedbacks as reasons for concern[23,24]. Here, we attempt to advance current understanding by isolating biophysical and biogeochemical feedbacks within a representative CMIP5 ensemble using the results from two experimental scenarios: fully coupled model simulations driven by prescribed [CO_2], climate, and land use change forcing for the historical and RCP8.5 scenario periods[2,3] ($CMIP5_{CO_2+CLIM}$; Supplementary Table 1); and radiatively coupled model simulations driven by the same forcing as the fully coupled simulations but in which the vegetation does not respond to increasing [CO_2] for the historical and RCP8.5 scenario periods[2,3] ($CMIP_{CLIM}$; Supplementary Table 1). We then evaluate the relative strength of biophysical and biogeochemical feedbacks represented in the CMIP5 ensemble against NPP estimates from satellite and ground observations.

Satellites provide high spatiotemporal resolution, global coverage of multiple facets of vegetation dynamics including photosynthetic capacity (that is, the fraction of photosynthetically active radiation absorbed by the vegetation; FPAR), leaf area index (LAI), and vegetation water content of above-ground biomass (that is, vegetation optical depth; VOD), which have been shown to strongly relate to vegetation productivity[9–11]. We used the Moderate Resolution Imaging Spectroradiometer (MODIS) NPP algorithm[9,10], driven by long-term Global Inventory Modeling and Mapping Studies (GIMMS) FPAR and LAI data[11], to calculate a new 30-year global data set of satellite-derived NPP (1982–2011). To account for potential bias introduced by the algorithm, we generated uncertainty bounds across a wide range of parameter combinations (see Methods). We further compare our results against a global eddy covariance flux-derived NPP data set[26,27] (Flux MTE; 1982–2008; Methods); and an independent satellite-derived VOD data product that is less prone to saturation in dense canopies

[1]Department of Ecosystem and Conservation Sciences, University of Montana, Missoula, Montana 59812, USA. [2]Institute on the Environment, University of Minnesota, St Paul, Minnesota 55108, USA. [3]Southwest Biological Science Center, US Geological Survey, Moab, Utah 86001, USA. [4]Department of Ecology and Evolutionary Biology, Princeton University, Princeton, New Jersey 08544, USA. [5]National Center for Atmospheric Research, Boulder, Colorado 80307, USA. [6]Institute for Arctic and Alpine Research, University of Colorado, Boulder, Colorado 80309, USA. [7]ARC Centre of Excellence for Climate Systems Science & Climate Change Research Centre, University of New South Wales, Sydney, New South Wales 2052, Australia. *e-mail: wkolby@gmail.com

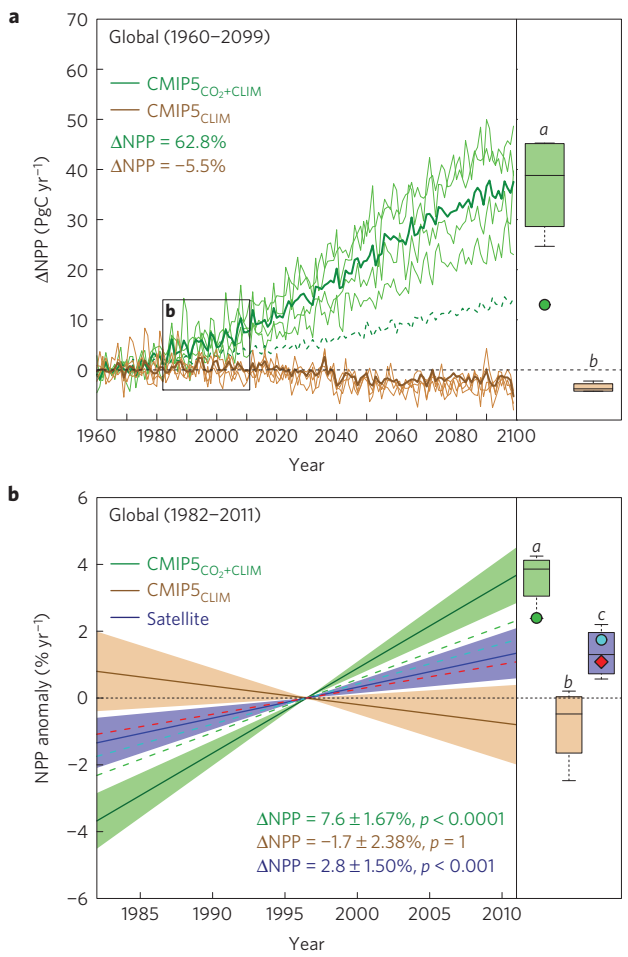

Figure 1 | Temporal changes in NPP. a, The change in NPP from 1960 to 2099. Heavy lines represent the ensemble mean for each CMIP5 experiment. **b**, The NPP anomaly from 1982 to 2011. Lines represent linear trends and shading indicates uncertainty ($\pm 1\sigma$) due to among-model variability for CMIP5 and model parameterization for satellite estimates. Box and whisker plots (right panels), show the distribution of estimates for the full time period. For comparison, the CMIP5 model that considered nutrient constraints (CESM1-BGC; dashed green line; green circle), Flux MTE (dashed red line; red diamond), and satellite FPAR (dashed cyan line; cyan circle) are shown separately. Letters indicate statistically significant differences in distributions at $\alpha = 0.05$.

and highly sensitive to changes in vegetation water content[28] (1988–2008; see Methods). By considering multiple independent observation-based data sets, we provide a robust characterization of long-term changes in global vegetation productivity.

By the end of the twenty-first century, the ensemble mean NPP for fully coupled simulations that included the response of vegetation to increasing [CO_2] ($CMIP5_{CO_2+CLIM}$) increased by roughly 63%, whereas the ensemble mean NPP for radiatively coupled simulations that included only the radiative effects of changes in [CO_2] ($CMIP5_{CLIM}$) decreased by roughly 6% (Fig. 1a and Supplementary Fig. 1). Over the period of satellite observation (1982–2011), a similarly strong positive CO_2 fertilization effect persists in CMIP5 NPP estimates; $CMIP5_{CO_2+CLIM}$ NPP estimates significantly increased ($7.6 \pm 1.67\%$), whereas $CMIP_{CLIM}$ NPP estimates did not significantly change ($-1.7 \pm 2.38\%$). Interestingly, satellite-derived NPP estimates increased over this period by $2.8 \pm 1.50\%$, a rate of change significantly different from either CMIP5 scenario (Fig. 1b). These satellite-derived NPP trends are largely consistent with long-term Flux MTE NPP and satellite VOD trends (Fig. 1b and Supplementary Fig. 2). The differences in CMIP5 and satellite-derived NPP trends are not a localized phenomenon, but are apparent along a global latitudinal gradient (Fig. 2) and across global climatic zones and biomes (Supplementary Figs 2 and 3). Thus, after taking into account among-model variability in the CMIP5 ensemble and model uncertainty in the satellite estimates (see Methods), the CMIP5 ESMs show significantly stronger global-scale CO_2 fertilization effects on NPP compared with satellite-derived estimates.

Why is the relatively strong CO_2 fertilization effect simulated by the CMIP5 ensemble not observed in the satellite-based record? One potential explanation could be differences in the sensitivity of NPP estimates to changing climatic constraints. In general, CMIP5 and satellite-based climate data show warming (that is, increasing minimum temperatures (TMIN)) and drying (that is, increasing atmospheric moisture demand or vapour pressure deficit (VPD)) trends that occur in parallel with increasing atmospheric [CO_2] (Supplementary Fig. 4). Hotter and dryer climatic conditions resulting from rising [CO_2] are known to increase vegetation moisture stress and reduce NPP (refs 16–20). Indeed, both CMIP5 and satellite-derived NPP estimates were found to be significantly negatively correlated with TMIN and VPD over large regions, suggesting that vegetation productivity is negatively impacted by increasing atmospheric moisture demand (Supplementary Figs 5 and 6). Yet, particularly in arid and temperate ecosystems, the relatively large negative effects of increasing atmospheric moisture demand are more than compensated for by even larger positive effects of CO_2 fertilization, resulting in an apparent insensitivity of $CMIP5_{CO_2+CLIM}$ NPP trends to increasing VPD (Supplementary Figs 2 and 4). Thus, CMIP5 and satellite NPP estimates seem to be diverging partially owing to differential sensitivity to the compensatory effects of increasing atmospheric [CO_2] and moisture demand.

To further explore the interacting effects of increasing atmospheric [CO_2] and moisture demand on vegetation productivity, we calculated the unit change in NPP per unit change in VPD using a sliding window of 10 years (Fig. 3). In theory, increasing atmospheric [CO_2] could drive static or decreasing sensitivity to VPD if the positive effects of CO_2 fertilization and increasing WUE are larger than the negative effects of moisture stress on NPP. This type of response would be characterized by relative increases in NPP in years of both low and high atmospheric moisture demand, resulting in constant or reduced inter-annual variability of NPP. Alternatively, sensitivity to VPD could increase if the negative effects of moisture stress are larger than the positive effects of CO_2 fertilization and increasing WUE on NPP. This type of response would be characterized by relative reductions in NPP in years of high atmospheric moisture demand and relative increases in NPP in years of low atmospheric moisture demand, resulting in increased inter-annual variability of NPP. For CMIP5 NPP estimates, we find a response similar to the former, relatively constant VPD sensitivity across all ecosystems, resulting in constant or reduced inter-annual variability in CMIP5 NPP estimates (Fig. 3 and Supplementary Fig. 7). In contrast, for satellite-derived NPP estimates, we found a response similar to the latter, significant increases in VPD sensitivity for arid ($4.7 \pm 1.24\%$, $P < 0.0001$) and temperate ($2.3 \pm 1.35\%$, $P < 0.01$) ecosystems as well as significant increases in inter-annual variability of NPP estimates across arid ecosystems ($7.0 \pm 2.27\%$, $P < 0.0001$) (Fig. 3 and Supplementary Fig. 8). Field experiments conducted in arid and temperate grassland ecosystems support these satellite-derived trends, and have shown that positive CO_2 fertilization effects on NPP are apparent in wet years, but not in years when moisture constraints are relatively strong[19]. These findings are consistent with work showing increased sensitivity of C uptake to precipitation across Australian semi-arid ecosystems[17], and add to a growing

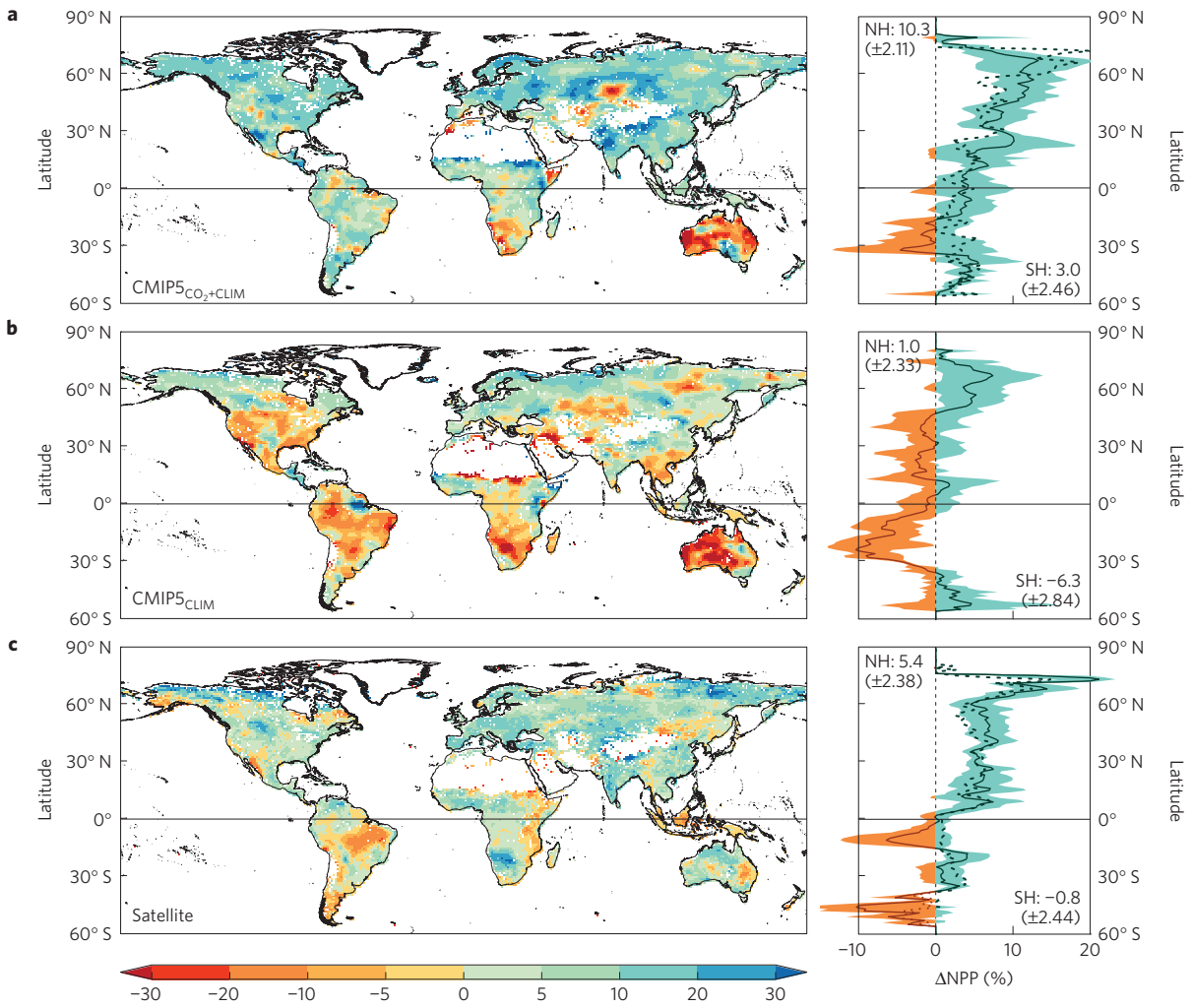

Figure 2 | Spatial and latitudinal changes in NPP from 1982 to 2011. a, $CMIP5_{CO_2+CLIM}$ NPP. **b**, $CMIP5_{CLIM}$ NPP. **c**, Satellite-derived NPP. In the latitudinal plots (right panels), shading indicates uncertainty ($\pm 1\sigma$) due to among-model variability for CMIP5 and model parameterization for satellite estimates. For comparison, the CMIP5 model that considered nutrient constraints (CESM1-BGC; top right panel, dashed line) and satellite FPAR (bottom right panel, dashed line) are shown separately. Values represent the average percentage change in NPP ($\pm 1\sigma$) for the Northern Hemisphere (NH) and Southern Hemisphere (SH) for the full time period.

body of evidence that suggests temperate and arid ecosystems have largely contributed to recent increases in the inter-annual variability of the terrestrial C cycle[17,18]. The significant differences in VPD sensitivity of CMIP5 and satellite NPP estimates provide insight into the divergent NPP trends, and highlight the need for research aimed at untangling the complex relationship between vegetation moisture stress and CO_2 fertilization effects, particularly in arid and temperate ecosystems.

Another potential explanation for differences between satellite and CMIP5 NPP trends is that the CO_2 fertilization effect could be constrained by nutrient availability[21–25], a factor implicit in satellite estimates but largely missing from CMIP5 simulations. Nutrient gradients have been detected in satellite indices at the global scale, and areas with relatively low nutrient availability show correspondingly low maximum vegetation greenness[29]. By isolating the CMIP5 model in the ensemble that includes N cycling (CESM1-BGC; Supplementary Fig. 1), we show that NPP trends are reduced by roughly a factor of two and align well with satellite estimates (Fig. 1b and Supplementary Fig. 2). Although we were able to consider only one model, our findings are supported by free-air CO_2 enrichment (FACE) experiments that include fertilization plots[14,17,21,22] and by a recent modelling study that showed a similar attenuation of NPP due to nutrient constraints for a full ensemble of CMIP5 models[23].

We further explored NPP sensitivity to atmospheric [CO_2] by comparing CMIP5 and satellite-derived NPP estimates with available FACE NPP data[12–15]—the most comprehensive field-based experimental data assessing the response of NPP to elevated [CO_2] (Supplementary Table 2). Across multiple global biomes, we found that CMIP5 NPP estimates are generally two to three times more sensitive to atmospheric [CO_2] compared with FACE NPP data; whereas CESM1-BGC, satellite-derived, and Flux MTE NPP estimates are similarly sensitive to atmospheric [CO_2] compared to FACE NPP data. (Fig. 4). The importance of nutrient constraints on NPP are emphasized by recent work suggesting that much of the CO_2 fertilization effect initially observed at FACE sites may represent a transient phenomenon that slows over time owing to the depletion of soil nutrients[14,21,22]. Although improvements in model representation of nutrient constraints are still critically needed, the implementation of nutrient constraints in ESMs could result in improved CO_2 sensitivity that better matches that of observation-based estimates[14,30].

Terrestrial NPP plays a fundamental role in regulating the global C cycle and the discord between observational-based estimates

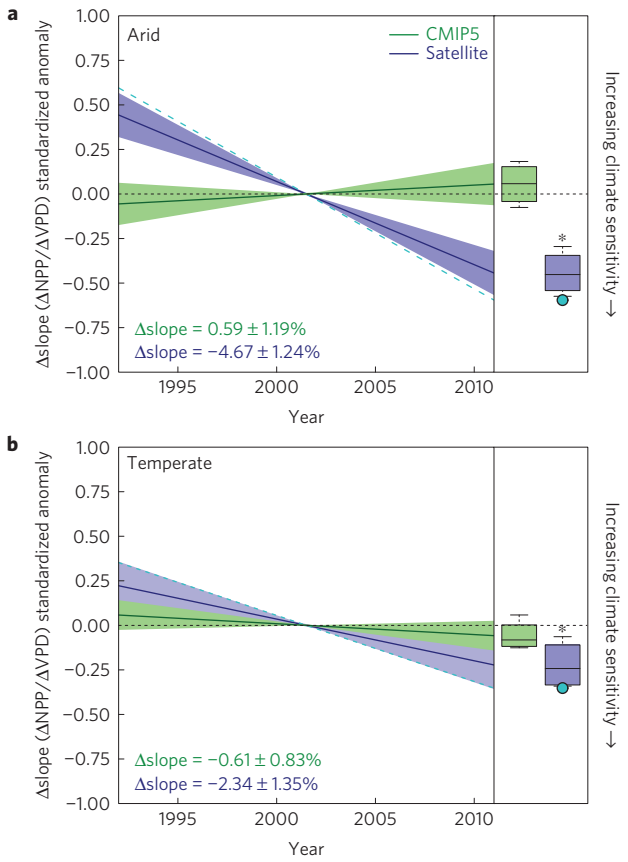

Figure 3 | The sensitivity of NPP to VPD. a,**b**, The change in NPP per unit change in VPD was calculated for arid (**a**) and temperate (**b**) climatic zones using a sliding window of 10 years. Shading indicates uncertainty ($\pm 1\sigma$) due to among-model variability for CMIP5 and model parameterization for satellite estimates. Box and whisker plots (right panels) show the distribution of estimates for the full time period. For comparison, the change in FPAR per unit change in VPD (cyan dashed lines) is shown separately. Asterisks indicate statistically significant differences in distributions from zero at $\alpha = 0.05$.

and model simulations is disconcerting. The large divergence of satellite-derived and ESM NPP estimates suggests that our understanding of CO_2 fertilization effects on terrestrial ecosystems is inadequate or not fully incorporated into ESMs, limiting our ability to accurately represent future C cycle–climate feedbacks. If satellite-based NPP estimates and field CO_2 experiments realistically reflect terrestrial ecosystem responses to increasing atmospheric [CO_2], the results would substantially alter projections of future terrestrial C storage and thus climate change, and suggest the need to reconsider allowable anthropogenic CO_2 emissions to achieve future climate change targets.

Methods

Methods and any associated references are available in the online version of the paper.

Received 23 December 2014; accepted 2 October 2015; published online 7 December 2015

References

1. Ballantyne, A. P., Alden, C. B., Miller, J. B., Tans, P. P. & White, J. W. C. Increase in observed net carbon dioxide uptake by land and oceans during the past 50 years. *Nature* **488**, 70–72 (2012).
2. Arora, V. K. *et al*. Carbon–concentration and carbon–climate feedbacks in CMIP5 Earth System Models. *J. Clim.* **26**, 5289–5314 (2013).

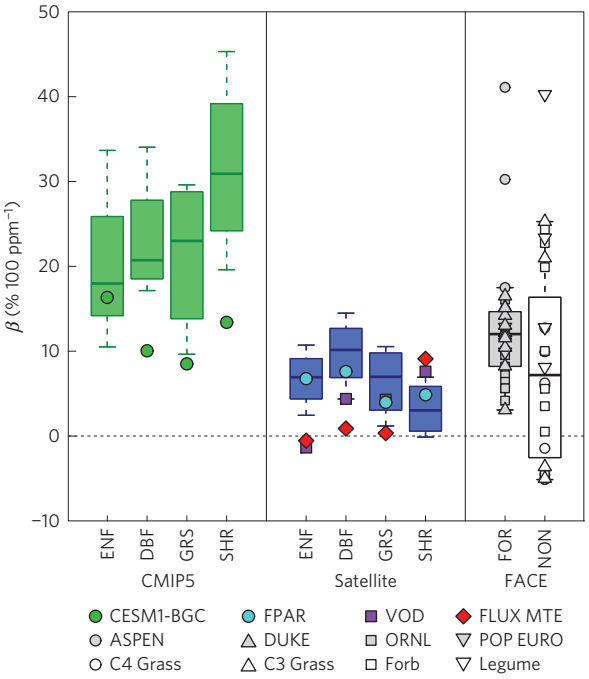

Figure 4 | The sensitivity of NPP to atmospheric [CO_2]. The change in NPP per 100 ppm change in CO_2 (β) was calculated for Northern Hemisphere evergreen (ENF) and deciduous (DBF) forests as well as temperate and arid grassland (GRS) and shrubland (SHR) ecosystems. We aggregated FACE β factors into forest (FOR; site-years = 28) and non-forest (NON; site-years = 32) distributions owing to the limited number of available FACE site-years (Supplementary Table 2).

3. Friedlingstein, P. *et al*. Uncertainties in CMIP5 climate projections due to carbon cycle feedbacks. *J. Clim.* **27**, 511–526 (2014).
4. Friend, A. D. *et al*. Carbon residence time dominates uncertainty in terrestrial vegetation responses to future climate and atmospheric CO_2. *Proc. Natl Acad. Sci. USA* **111**, 3280–3285 (2014).
5. Sitch, S. *et al*. Evaluation of the terrestrial carbon cycle, future plant geography and climate-carbon cycle feedbacks using five Dynamic Global Vegetation Models (DGVMs). *Glob. Change Biol.* **14**, 2015–2039 (2008).
6. Piao, S. *et al*. Evaluation of terrestrial carbon cycle models for their response to climate variability and to CO_2 trends. *Glob. Change Biol.* **19**, 2117–2132 (2013).
7. Schimel, D., Stephens, B. B. & Fisher, J. F. Effects of increasing CO_2 on the terrestrial carbon cycle. *Proc. Natl Acad. Sci. USA* **112**, 436–441 (2014).
8. Keenan, T. F. *et al*. Increase in forest water-use efficiency as atmospheric carbon dioxide concentrations rise. *Nature* **499**, 324–327 (2013).
9. Zhao, M. & Running, S. W. Drought-induced reduction in global terrestrial net primary production from 2000 through 2009. *Science* **1667**, 2–5 (2010).
10. Running, S. W. *et al*. A continuous satellite-derived measure of global terrestrial primary production. *Bioscience* **54**, 547–560 (2004).
11. Zhu, Z., Bi, J., Pan, Y., Ganguly, S. & Anav, A. Photosynthetically active radiation (FPAR) 3g derived from global inventory modeling and mapping studies (GIMMS) normalized difference vegetation index. *Remote Sens.* **5**, 927–948 (2013).
12. Norby, R. J. *et al*. Forest response to elevated CO_2 is conserved across a broad range of productivity. *Proc. Natl Acad. Sci. USA* **102**, 18052–18056 (2005).
13. Reich, P. B. *et al*. Do species and functional groups differ in acquisition and use of C, N and water under varying atmospheric CO_2 and N availability regimes? A field test with 16 grassland species. *New Phytol.* **150**, 435–448 (2001).
14. Zaehle, S. *et al*. Evaluation of 11 terrestrial carbon–nitrogen cycle models against observations from two temperate free-Air CO_2 enrichment studies. *New Phytol.* **202**, 803–822 (2014).
15. Morgan, J. A. *et al*. C4 grasses prosper as carbon dioxide eliminates desiccation in warmed semi-arid grassland. *Nature* **476**, 202–205 (2011).
16. Donohue, R. J., Roderick, M. L., McVicar, T. R. & Farquhar, G. D. Impacts of CO_2 fertilization on maximum foliage cover across the globe's warm, arid environments. *Geophys. Res. Lett.* **40**, 1–5 (2013).
17. Poulter, B. *et al*. Contribution of semi-arid ecosystems to interannual variability of the global carbon cycle. *Nature* **509**, 600–603 (2014).

18. Ahlström, A. *et al*. The dominant role of semi-arid ecosystems in the trend and variability of the land CO_2 sink. *Science* **348**, 895–899 (2015).
19. Reich, P. B., Hobbie, S. E. & Lee, T. D. Plant growth enhancement by elevated CO_2 eliminated by joint water and nitrogen limitation. *Nature Geosci.* **7**, 920–924 (2014).
20. Williams, A., Allen, C. & Macalady, A. Temperature as a potent driver of regional forest drought stress and tree mortality. *Nature Clim. Change* **3**, 292–297 (2013).
21. Norby, R. J., Warren, J. M., Iversen, C. M., Medlyn, B. E. & Mcmurtrie, R. E. CO_2 enhancement of forest productivity constrained by limited nitrogen availability. *Proc. Natl Acad. Sci. USA* **107**, 19368–19373 (2010).
22. Oren, R. *et al*. Soil fertility limits carbon sequestration by forest ecosystems in a CO_2-enriched atmosphere. *Nature* **411**, 469–472 (2001).
23. Wieder, W. R. *et al*. Future productivity and carbon storage limited by terrestrial nutrient availability. *Nature Geosci.* **8**, 441–444 (2015).
24. Hungate, B. A., Dukes, J. S., Shaw, M. R., Luo, Y. & Field, C. B. Nitrogen and climate change. *Science* **302**, 1512–1513 (2003).
25. Cleveland, C. C. *et al*. Patterns of new versus recycled primary production in the terrestrial biosphere. *Proc. Natl Acad. Sci. USA* **110**, 1–5 (2013).
26. Beer, C. *et al*. Terrestrial gross carbon dioxide uptake: global distribution and covariation with climate. *Science* **329**, 834–838 (2010).
27. Jung, M. *et al*. Global patterns of land-atmosphere fluxes of carbon dioxide, latent heat, and sensible heat derived from eddy covariance, satellite, and meteorological observations. *J. Geophys. Res.* **116**, 1–16 (2011).
28. Liu, Y. Y. *et al*. Global vegetation biomass change (1988–2008) and attribution to environmental and human drivers. *Glob. Ecol. Biogeogr.* **22**, 692–705 (2013).
29. Fisher, J. B., Badgley, G. & Blyth, E. Global nutrient limitation in terrestrial vegetation. *Glob. Biogeochem. Cycles* **26**, GB3007 (2012).
30. Medlyn, B. E. *et al*. Using ecosystem experiments to improve vegetation models. *Nature Clim. Change* **5**, 528–534 (2015).

Acknowledgements

This work was supported by the US Geological Survey Ecosystems Mission Area, US Department of Energy Terrestrial Ecosystem Sciences Program (Award no. DE-SC-0008168), the US Geological Survey John Wesley Powell Center for Analysis and Synthesis, and the NASA Earth Observing System MODIS project (grant no. NNX08AG87A). Y.Y.L. is supported by an Australian Research Council DECRA Fellowship (project number DE140100200). We also acknowledge the World Climate Research Programme's Working Group on Coupled Modelling, which is responsible for CMIP, and we thank the climate modelling groups (listed in Supplementary Table 1 of this paper) for producing and making available their model output. For CMIP, the US Department of Energy's Program for Climate Model Diagnosis and Intercomparison provides coordinating support and led development of software infrastructure in partnership with the Global Organization for Earth System Science Portals. Any use of trade, firm, or product names is for descriptive purposes only and does not imply endorsement by the US Government. All data presented in this analysis are publicly available; satellite estimates are available at the NTSG data portal (http://www.ntsg.umt.edu/data); CMIP5 experimental scenario data are available at the ESGF data portal (http://esgf.llnl.gov).

Author contributions

W.K.S., S.C.R., C.C.C., A.P.B. and S.W.R. designed the study. W.K.S. carried out the analysis and wrote the paper. W.R.L.A. contributed to the climate sensitivity analysis. W.R.W. contributed to the nutrient limitation discussion. Y.Y.L. provided the vegetation optical depth data and helped with associated data interpretation. All authors contributed significantly to the final revisions of the manuscript.

Additional information

Supplementary information is available in the online version of the paper. Reprints and permissions information is available online at www.nature.com/reprints. Correspondence and requests for materials should be addressed to W.K.S.

Competing financial interests

The authors declare no competing financial interests.

Methods

Satellite NPP data. We used the MODIS NPP algorithm, driven by newly available 30-year (1982–2011) Global Inventory Modeling and Mapping Studies (GIMMS) FPAR and LAI data, to calculate a new 30-year global data set of satellite-derived gross primary productivity (GPP), net primary productivity (NPP), and autotrophic respiration[9–11] (RA):

$$\mathrm{NPP}=\sum_{i=1}^{t}[\mathrm{FPAR}_i\times\mathrm{IPAR}_i\times\mathrm{LUE}_{\max}\times f(\mathrm{VPD}_i)\times f(\mathrm{TMIN}_i)-\mathrm{RA}_i]$$

where FPAR represents the satellite-derived fraction of photosynthetically active radiation absorbed by the vegetation, IPAR represents the incoming photosynthetically active radiation, $\mathrm{LUE}_{\max}$ represents biome-specific maximum light use efficiency, f(VPD) represents a water stress reduction scalar, f(TMIN) represents a low-temperature stress reduction scalar, and RA represents autotrophic respiration. $\mathrm{LUE}_{\max}$, f(VPD), f(TMIN) and RA were initially parameterized according to ref. 9. IPAR, TMIN, and VPD data were derived from NCEP-DOE Reanalysis II (http://www.esrl.noaa.gov). VPD was computed as the difference between saturation and actual vapour pressure using daily temperature, surface pressure, and specific humidity variables according to the method used by ref. 9. All satellite NPP data were re-gridded to a common 1° global grid.

The MODIS NPP algorithm and the GIMMS FPAR and LAI data have been evaluated extensively against a wide range of observational data and model output, and have been found to generally provide realistic information on vegetation production across the global range of observed climates and biome types[9–11]. That said, NPP cannot be measured directly at large scales and satellite-derived NPP estimates are influenced by algorithm parameterization, especially in areas of dense evergreen forests (for example, tropical forests) where satellite FPAR and LAI indices can saturate[31,32]. To account for these challenges, we calculated uncertainty bounds that represent the full range of potential parameter combinations in the MODIS NPP algorithm, enabling a focus on the actual satellite signal. Climate constraints f(VPD) and f(TMIN) were thus allowed to range from optimized (parameterization derived from ref. 9) to a fixed mean value resulting in the simplified equation:

$$\mathrm{NPP}=\sum_{i=1}^{t}[\mathrm{FPAR}_i\times\mathrm{IPAR}_i\times\mathrm{LUE}_{\max}\times f(\overline{\mathrm{VPD}})\times f(\overline{\mathrm{TMIN}})-\mathrm{RA}_i]$$

The full range of variability in autotrophic respiration and its influence on NPP trends was captured using two independent RA approximations: a temperature sensitivity (that is, non-acclimation) approach, by which RA was calculated using a Q_{10} function that is sensitivity to changes in average temperature, implemented according to ref. 9; and an acclimation approach, by which RA was calculated simply as a fixed ratio of GPP, resulting in the further simplified equation:

$$\mathrm{NPP}=\sum_{i=1}^{t}[\mathrm{FPAR}_i\times\mathrm{IPAR}_i\times\mathrm{LUE}_{\max}\times f(\overline{\mathrm{VPD}})\times f(\overline{\mathrm{TMIN}})\times\mathrm{RA}_{\mathrm{scalar}}]$$

where $\mathrm{RA}_{\mathrm{scalar}}$ represents the constant fraction of GPP (0.5) that is respired through maintenance and growth respiration. This simplified representation of RA best matched that of the CMIP5 models, which were generally found to model GPP and RA as tightly coupled for the full temporal extent of the study. See ref. 9 for additional algorithm detail.

Flux MTE and satellite VOD data. We included 27-year eddy covariance flux-based NPP data, derived from a diagnostic model calibrated using global flux site-level data by means of a model tree ensemble machine learning technique (1982–2008; Flux MTE; refs 26,27) as a largely independent observation-based vegetation production data set. Flux MTE data were converted from GPP to NPP using a fixed ratio (0.5). We also included 21-year (1988–2008) satellite vegetation optical depth (VOD; that is, an indicator of vegetation water content of above-ground biomass, including leaf and woody components) data as an independent observation-based indicator of vegetation production[28]. VOD is derived from passive microwave remote sensing and is less prone to saturation and atmospheric effects. VOD is, however, less reliable in areas with substantial open water bodies, and it is not available when the surface temperature is below 0° or in the presence of snow. Thus, we limit our VOD analyses to regions without substantial open water bodies and we consider only summertime (July–September) months when examining forests in high latitudes of the Northern Hemisphere. Finally, to better reflect net annual change, we base our analyses on ΔVOD (that is, the annual difference in VOD).

CMIP5 NPP data. Data from individual ESMs were downloaded from the CMIP5 archive (Supplementary Table 1). These data included NPP, GPP and RA (land variables) as well as TMIN and VPD (atmospheric variables). VPD was computed as the difference between saturation and actual vapour pressure using daily temperature, surface pressure, and specific humidity variables according to the method used by ref. 9. Data from the 'historical' and RCP8.5 scenario periods[2,3] were combined to generate continuous variable fields from 1960 to 2099. We used all ESMs with complete data records included in the esmFdbk2 experiment—in which the carbon cycle sees pre-industrial (control) atmospheric $[CO_2]$, whereas the radiation code sees observed increases. The CMIP5 ensemble thus included five members and variability was calculated as one standard deviation ($\pm1\sigma$) of the mean (Supplementary Fig. 1). It is important to note that we focus this analysis on 30-year trends, not inter-annual variability in NPP, because the CMIP5 model runs considered in this study were not forced by climate data and instead started from an arbitrary point of a quasi-equilibrium control run, resulting in inter-annual variability that does not, and should not, be expected to align with the observational record. All CMIP5 data were re-gridded to a common 1° global grid using the bilinear method of interpolation.

Free-air CO_2 enrichment (FACE) comparison. Data from FACE experiments were used to evaluate model sensitivity to atmospheric $[CO_2]$ (refs 12–15). Site locations and characteristics can be found in Supplementary Table 2. Two approaches were used to estimate the sensitivity of NPP to atmospheric $[CO_2]$ (β; that is, the change in NPP per 100 ppm change in CO_2). For FACE NPP estimates, β was calculated by isolating the CO_2 fertilization effect:

$$\beta=\frac{\Delta\mathrm{NPP}}{\Delta\mathrm{CO}_2}$$

where ΔNPP represents the difference between NPP measured under elevated and ambient CO_2 treatments. ΔCO_2 represents the corresponding change in atmospheric $[CO_2]$ (Fig. 4).

For CMIP5 and satellite estimates, a multiple regression approach was used and β factors were calculated according to the general linear model:

$$\mathrm{NPP}=\beta(\mathrm{CO}_2)+C1(\mathrm{VPD})+C2(\mathrm{TMIN})+C3+\varepsilon$$

where NPP represents the NPP time series, and CO_2, VPD and TMIN represent the atmospheric $[CO_2]$, vapour pressure deficit and the minimum temperature time series for each model, respectively. β, $C1$, $C2$ and $C3$ represent regression coefficients and ε is the residual error term. Regression coefficient β was estimated using maximum likelihood analysis. As we were interested in relative differences, it is unlikely that the inclusion of other confounding drivers (for example, precipitation and radiation) would greatly change the conclusions of this analysis.

Statistical analyses. Linear correlation coefficients (Pearson's R) were calculated to quantify the concurrent association between time series. Time series data were detrended before correlation analyses to account for potential auto-correlation among variables. Trend and maximum likelihood estimates were calculated using the lm() function in R 2.11.1 (R development Core team). Sliding trends were calculated as the change in the trend over a 10-year sliding window using the lm() function in R 2.11.1. Statistical significance (P values) were estimated throughout this analysis using a two-factor analysis of variance (ANOVA) and Tukey's HSD (ANOVA() and TukeyHSD() functions in R 2.11.1) or a Student's t-test (t.test() function in R 2.11.1) for pair-wise differences. Comparisons across land-cover types and climate zones were defined using the MODIS collection 5 global land-cover classification (https://lpdaac.usgs.gov/dataset_discovery/modis/modis_products_table; ref. 33) and the Köppen–Geiger climate zones classification (http://people.eng.unimelb.edu.au/mpeel/koppen.html; ref. 34).

Limitations and potential missing mechanisms. We do not explicitly consider the effects of disturbance[35] or shifting land cover[36] on NPP; factors implicit in satellite-derived NPP estimates but missing from CMIP models. Although these factors could have important local effects in some regions, it is unlikely that they explain the large-scale observed differences in CMIP5 and satellite-derived NPP trends.

Our comparison against field-based experimental data is limited in tropical regions where differences in NPP and uncertainty are greatest[37,38] (Supplementary Fig. 2). Quality remote sensing data from tropical regions are also limited owing to saturation effects as well as frequent cloud and aerosol contamination[28,31,32]. Still, trends in satellite VOD data—relatively insensitive to saturation and cloud effects—are slightly negative for tropical ecosystems over the 1988–2008 observation period, suggesting that any positive CO_2 fertilization effects are ameliorated by or even secondary to negative climate and/or land use change effects on NPP (refs 28,31,32; Supplementary Fig. 2). This finding is supported by a recent analysis of tropical tree growth rings that found no evidence for growth simulation due to CO_2 fertilization[39] as well as a long-term field study that found negative climate effects far exceed slight positive CO_2 fertilization effects on NPP for a tropical forest site[40].

NPP and terrestrial carbon storage. Global-scale atmospheric $[CO_2]$ measurements and estimated trends in terrestrial carbon storage are a common benchmark for CMIP5 models[1,41]. Holding all factors equal, reduced rates of NPP

would result in an underestimation of historical C uptake and an overestimation of atmospheric [CO_2] in CMIP5 models. However, this apparent discrepancy can be easily reconciled by realistically modified C turnover times, as demonstrated by a recent study[23]. Using a multiple optimization framework that considers atmospheric CO_2 measurements, CO_2 emission estimates, and satellite-derived NPP trends could improve ESM performance and provide key insight into the potential impact of climate change on C turnover times[4,42].

References

31. Hilker, T. *et al*. Vegetation dynamics and rainfall sensitivity of the Amazon. *Proc. Natl Acad. Sci. USA* **111**, 16041–16046 (2014).
32. Zhou, L. *et al*. Widespread decline of Congo rainforest greenness in the past decade. *Nature* **509**, 86–90 (2014).
33. Friedl, M. A. *et al*. MODIS Collection 5 global land cover: Algorithm refinements and characterization of new datasets. *Remote Sens. Environ.* **114**, 168–182 (2010).
34. Peel, M. C., Finlayson, B. L. & McMahon, T. A. Updated world map of the Köppen–Geiger climate classification. *Hydrol. Earth Syst. Sci.* **11**, 1633–1644 (2007).
35. Liu, Y. Y. *et al*. Recent reversal in loss of global terrestrial biomass. *Nature Clim. Change* **5**, 470–474 (2015).
36. Koven, C. D. Boreal carbon loss due to poleward shift in low-carbon ecosystems. *Nature Geosci.* **6**, 452–456 (2013).
37. Cleveland, C. C. *et al*. A comparison of plot-based, satellite and Earth system model estimates of tropical NPP. *Glob. Biogeochem. Cycles* **21**, 2111–2121 (2015).
38. Cavaleri, M. A., Reed, S. C., Smith, W. K. & Wood, T. E. Urgent need for warming experiments in tropical forests. *Glob. Change Biol.* **29**, 626–644 (2015).
39. Van der Sleen, P. *et al*. No growth stimulation of tropical trees by 150 years of CO_2 fertilization but water-use efficiency increased. *Nature Geosci.* **8**, 24–28 (2015).
40. Clark, D. A., Clark, D. B. & Oberbauer, S. F. Field-quantified responses of tropical rainforest aboveground productivity to increasing CO_2 and climatic stress, 1997–2009. *J. Geophys. Res.* **118**, 783–794 (2013).
41. Hoffman, F. M. *et al*. Causes and implications of persistent atmospheric carbon dioxide biases in Earth System Models. *J. Geophys. Res.* **119**, 141–162 (2014).
42. Carvalhais, N. *et al*. Global covariation of carbon turnover times with climate in terrestrial ecosystems. *Nature* **514**, 213–217 (2015).